AS861.TEX ASME86

NEW MODELS AND METHODOLOGY FOR PREDICTING THERMAL CONTACT RESISTANCE IN COMPOUND CYLINDERS AND FIN-TUBES

T. F. Lemczk, Graduate Research Assistant and M. M. Yovanovich, Professor
Thermal Engineering Group
Department of Mechanical Engineering
University of Waterloo
Waterloo, Ontario, Canada

ABSTRACT

New thermal conductance correlations based on improved metal, gap, and joint contact models are presented for determining the thermal interfacial resistance in compound cylinders. The new theory utilizes models involving measured surface parameters, material hardness, thermophysical properties and iteratively evaluated contact stresses.

Differences in the proposed theory compared to previously employed models include the measure of Vickers microhardness which has proven to yield very accurate results in recently published experimental investigations by Yovanovich and coworkers. Also, the interfacial gap conductance is correlated to be indirectly a function of the contact pressure. This differs from the models proposed by several previous investigators (Ross & Stoute, Shlykov & Ganin, Veziroglu) who assumed the gap resistance to be independent of contact pressure. The total joint conductance is then defined as a sum of the gap and metal contact conductances.

Employing these new contact and gap correlations, the proposed methodology determines the operating contact pressures through an iterative procedure which 'couples' the heat transfer to the classical thermoelastic stress analysis of the materials. This differs from previous methods, in which the heat transfer and mechanical analyses were essentially treated separately.

The predictions of previous and proposed models are compared to recently published experimental investigations on compound cylinders. Accuracy to within 5% of experimental data is obtained by means of the proposed models. It was found that the alternative models grossly overestimated the thermal contact resistance in compound cylinders, with error ranges from 25% to 100% (Ross & Stoute and Shlykov & Ganin) and 100 to 200% (Veziroglu) of the experimental results. The experimental verifications thereby support the new models in the analysis of compound cylinders, with direct applications in analysing the performance of fin-tube heat exchangers.

NOMENCLATURE

a	- inner cylinder radius
A	- subscript used to denote inner cylinder parameters
b	- interfacial radius
B	- subscript used to denote outer cylinder parameters
B_1, B_2, B_3, B_4	- mechanical integration constants
Bi	- Biot Number $\equiv ht/k$ (fin)
c	- outer cylinder or fin radius
C_1, C_2, C_3, C_4	- thermal integration constants
E, E_A, E_B	- elastic modulus, moduli of inner and outer cylinders
h, h_i, h_o, h_e	- convective film conductance on fin, inner system, outer (cyl.) system, and end of fin
h_c, h_g, h_j	- metal, gap and total joint conductance
H, H_e	- bulk and effective microhardness
I_o, I_1	- modified Bessels functions of the first kind, orders 0 and 1
K_o, K_1	- modified Bessels functions of the second kind, orders 0 and 1
k_1, k_2, k_A, k_B	- thermal conductivities of specimens 1 and 2, or A and B
k_s	- harmonic mean thermal conductivity $= 2k_1k_2/(k_1 + k_2)$
k_{go}	- gap gas thermal conductivity
m	- effective absolute surface slope $= \sqrt{m_1^2 + m_2^2}$

M	- gas parameter $= \alpha\beta\Lambda/\sigma$
P_i, P_o	- internal and external system pressures (negative compressive)
P_c^i, P_c^{SH}, P_c	- initial (manufactured), shrink-fit, and final operating contact pressures
P_g, P_{go}	- gap gas pressure and reference gas pressure
Pr	- Prandtl Number
r	- radius
R_c, R_g, R_j	- metal, gap and joint resistances defined as $h_c^{-1}, h_g^{-1}, h_j^{-1}$ respectively
t	- fin half-thickness
T, T_A, T_B	- temperature, inner and outer cylinder temperatures
T_m, T_{mo}	- gap gas mean temperature and reference mean gap temperature
T_i, T_o, T_{ref}	- inner, outer and reference system temperature
u, u_A, u_B	- radial displacement of cylinders A,B and fin
Y	- mean plane separation

Greek Symbols

$\alpha, \alpha_A, \alpha_B$	- linear thermal coefficients of expansion
$\alpha_1, \alpha_2, \alpha_a$	- accommodation coefficients and accommodation parameter
β	- fluid parameter
γ	- gap gas specific heat ratio $= C_p/C_v$
δ	- radial shrink-fit difference
$\Delta T(r)$	- differential thermal expansion temperature $= T(r) - T_{ref}$
$\epsilon_{rr}, \epsilon_{\theta\theta}, \epsilon_{zz}$	- radial and circumferential strains
Λ, Λ_o	- molecular mean free path, and reference mean free path
ν, ν_A, ν_B	- Poisson's ratio for materials
$\sigma_A, \sigma_B, \sigma$	- surface roughnesses and effective roughness
σ_{rr}	- radial stress

Note: several variables listed in Appendices III and IV are not included here for simplicity

INTRODUCTION

The thermal contact resistance at the interface of two curved surfaces becomes particularly important in the analysis of mechanically formed fin-tube heat exchangers and various cylindrical sheaths (i.e. nuclear pellets) exchanging heat. One of the first serious investigations into this subject, was conducted by Gardner and Carnavos [1], using a contact resistance model, which has since been significantly updated through numerous plane-contact studies [2-8]. The experimental study by Christensen and Fernandes [2] gave order of magnitude estimates for contact and fouling resistances, but no adequate correlation. Eckels [3] presented a model for mechanically expanded plate finned-tube heat exchangers, successfully predicting experimental effects of varying fin number, thickness and tube diameter. Unfortunately the model requires a least squares curve fit to a power relation between conductance and contact pressure. This is particularly inadequate for the large variation of parameters which occur, since it would require independent curve-fitting for each case. Kern and Kraus [4] discuss fin-bond analysis, utilizing models developed by Shlykov and Ganin [5], which are demonstrated by Hsu and Tam [6] and this study, to be inadequate when verified experimentally. Contact correlations developed by Yovanovich [7] and experimentally verified in plane-contact conditions [8] appear to be the most recent and accurate in the literature. The joint conductance is also a direct function of a Vickers microhardness distribution, which has been shown [9] to successfully predict conductance with various penetration depths. The penetration is due to the asperities (see Fig. 1) of contact between two conforming surfaces. It is clear from these studies that the effective microhardness will decrease with increasing depth of penetration.

The complete procedure of estimating the heat transfer and the elasticity solution for a double tube system has previously been considered independently. A new methodology is shown where the joint conductance being a function of contact pressure, is iteratively obtained through a combined thermal-elastic procedure. Convergence is guaranteed quickly due to the light non-linear relation between joint conductance and contact pressure in the proposed theory of Yovanovich [7].

The purpose of the present investigation is to accurately and systematically predict the thermal joint resistance at the interface of a typical double-tube system. Verification for the model is made by comparison with experimental results published by Hsu and Tam[6]. Parameters such as surface slope and effective hardness (Vickers) were estimated since these were not supplied through their report. The surface roughness of the aluminum cylinders varied over a range of 3 - 4.8 microns rms in the first set, and a range of 0.76 - 0.94 microns rms in the second set of their results. Using the maximum roughness of their specimens, (since this would be the controlling range) good verification to within 5% was achieved using the proposed theory. The thermal joint resistance predicted was substantially lower than predictions made by alternative models [6]. This was attributed to the inadequacy of those models, rather than thermal strain effects which do not affect the proposed contact correlation.

Finally, a typical fin-tube analysis is outlined analytically indicating the thermal flux effects on contact resistance variation at low contact pressures.

IMPROVED METAL, GAP AND JOINT CONDUCTANCE MODELS

The joint conductance models to be used here are based upon correlations developed by Yovanovich [7] and studies conducted into surface hardness distributions by Yovanovich et al [8,9,10]. These conductance correlations have been verified quantitatively in numerous experiments. Important assumptions concerning the geometric, physical and thermal aspects of the models can be found in detail in those publications, however, a few of these are now listed:

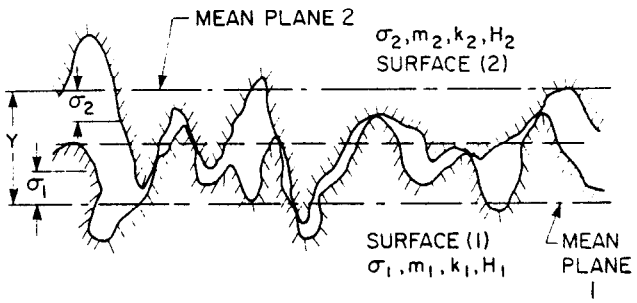

Fig.1 Typical Micro-profile of Two Conforming Contacting Surfaces

1. the surfaces are microscopically rough and macroscopically conforming.
2. the asperity heights are gaussian and the asperities are randomly distributed over the apparent contact area.
3. the contacting asperities deform plastically during the first loading (of the softer solid).
4. the effective gap thickness is dependent upon the surface roughness and the relative contact pressure.

The final proposed joint conductance h_j, for the imperfect contact of two surfaces shown in Fig. 1, can be approximately stated as a sum of the metal (contact) h_c, and gap, h_g, conductances:

$$h_j = h_c + h_g \tag{1}$$

where

$$h_c = 1.25\frac{k_s m}{\sigma}(P_c/H_e)^{0.95}, \tag{2}$$

$$h_g = \frac{k_{go}}{(Y + \alpha_a \beta \Lambda)} \tag{3}$$

The quantities k_s,m, σ, found in h_c, are defined as:

$$k_s = \frac{2k_1k_2}{k_1 + k_2} \tag{4}$$

$$\sigma = (\sigma_1^2 + \sigma_2^2)^{\frac{1}{2}} \tag{5}$$

$$m = (m_1^2 + m_2^2)^{\frac{1}{2}} \tag{6}$$

The parameters σ, m and $H = H_e$(the effective material microhardness based on the Vickers test for the softer of the two contacting metals) necessitate experimental measurement which will of course vary from sample to sample.

In the gap conductance h_g, the mean plane separation Y is correlated [7] as a direct function of σ and P_c:

$$Y = 1.184\sigma[-\ell n(3.132P_c/H_e)]^{0.547} \tag{7}$$

We also have the parameters α_a, β and Λ.

The accommodation parameter α_a, is defined as:

$$\alpha_a = \frac{2 - \alpha_1}{\alpha_1} + \frac{2 - \alpha_2}{\alpha_2} \tag{8}$$

where the accommodation coefficients α_1, α_2 are empirically determined [7]. The fluid parameter β is determined by

$$\beta = \left(\frac{2\gamma}{\gamma + 1}\right)\frac{1}{Pr} \tag{9}$$

Table 1 Typical Ranges of Parameters

10^{-5}	$<$	P_c/H_e	$<$	10^{-2}
4.26	$>$	Y/σ	$>$	2.34
$0.14\mu m$	$<$	σ	$<$	$14\mu m$
$9.33\mu m$	$<$	σ/m	$<$	$40\mu m$
.015	$<$	m	$<$	0.35
2	$<$	α_a	$<$	20
1	$<$	β	$<$	2
$0.04\mu m$	$<$	Λ_o	$<$	$0.19\mu m$
0.001	$<$	Λ_o/σ	$<$	1.5
10^{-4}	$<$	k_{go}/k_s	$<$	$2\,\text{x}10^{-2}$

ticular values of σ and m). This hardness is not to be confused with say the Brinell or Rockwell hardness measures which assume that there is an isotropic hardness throughout the surface asperities, and thus giving a general bulk value. This approach was found to be completely inadequate [8] for predicting contact conductances, therefore demonstrating the importance of the microhardness layer on the proposed conductance theory.

where γ is the specific heat ratio and Pr is the Prandtl number.

The molecular mean free path Λ is defined as a function of the gap gas mean temperature $T_m(K)$ and the gap gas pressure P_g:

$$\Lambda = \Lambda_o\left(\frac{T_m}{T_{mo}}\right)\left(\frac{P_{go}}{P_g}\right) \tag{10}$$

Typical ranges of the parameters reported thus far are shown in Table 1.

In review, the proposed joint conductance correlations require the experimental measurement of three parameters σ, m and H_e for both contacting metal surfaces. The remaining parameters may be evaluated from given material specifications and interstitial gas data. It is important to emphasize that the Vickers microhardness H_e is in fact based on a distribution [9,10] which is computed for a particular surface (i.e. for par-

THERMAL CONTACT RESISTANCE IN COMPOUND CYLINDERS

The proposed correlations were developed in a general plane sense for conforming rough surfaces. Typical test arrangements have been with flat-ended and rounded cylinders under end contact conditions. Concentric cylinder contacts were not previously used for these correlations.

Hsu and Tam [6] reported that two conventional plane-contact models (Shlykov–Ganin and modified Ross–Stoute) were inadequate in verifying their experimental results. In this section we verify the experimental results obtained by Hsu and Tam, using an iterative thermoelastic procedure utilizing our proposed joint conductance correlations and microhardness distributions. Note that throughout the following analyses, $R_j \equiv 1/h_j$ (in actual, $R_j = \frac{1}{h_j A}[K/W]$) as this was reported in [6].

The double-tube system to be studied is shown in Fig. 2, as reported by Hsu and Tam [6]. The inner hollow aluminum cylinder was cold-fitted into the outer hollow stainless steel cylinder. Pertinent system and material data as published, is shown in Table 2, for test #1. (Test TCR-1 from Ref. [6]).

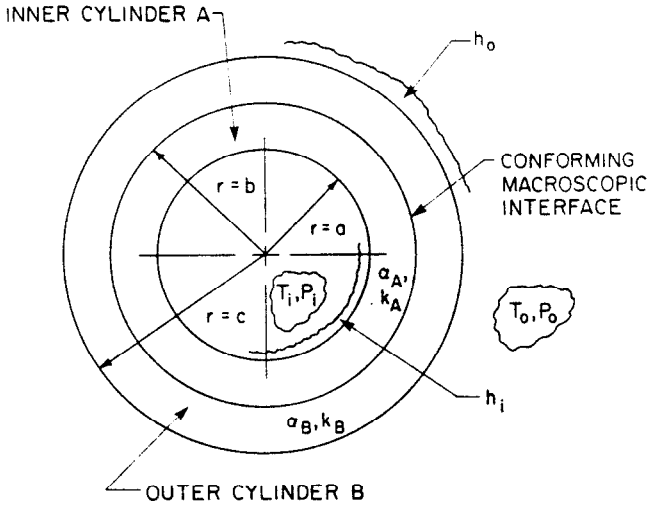

LENGTH OF COMPOUND SET: 144 mm
END FACES ARE RESTRAINED FROM EXPANSION

Fig.2 Typical Double-Tube System

Table 2 Specimen Descriptions, Ref. [6]

	Inner Cylinder A (2011-T351 Alclad)	Outer Cylinder B (304 Stainless)
I.D.(mm)	22.23	59.16
O.D.(mm)	59.16 - 59.19	72.52
$\sigma(\mu m)$	3.05 - 4.83	1.27 - 1.65
$k(W/mK)$	154.9	16.3
$E(MPa)$	7.10 x10^4	2.00 x10^5
$\alpha(K^{-1})$	2.28 x10^{-5}	1.728 x10^{-5}
$H(MPa)$	932	2420

In addition a second test was conducted with a roughness range of 0.762 - 0.940 μm for the inner cylinder and an outer cylinder O.D. of 72.44 mm. All other data for test #2 are identical to those shown in Table 2, for test #1.

The microhardness values reported by Hsu and Tam and shown in Table 2, were provided by the material manufacturers of their specimens. It is not reported which hardness measure was used, and for this reason new Vickers microhardness values are reported in Table 3. Calculation of these from their microhardness distributions can be found in Appendix I, (see also [8],[9],[10]). Also, estimated values of slope m for each specimen and interfacial gas (air) properties are included in Table 3.

For Test #2, the estimated surface slope range for the aluminum inner cylinder was 0.03, and the corresponding Vickers hardness used was 1.8 x10^3 MPa. This differs from that used for test #1(H_e = 1.2 x10^3 MPa) which illustrates the effect of asperity penetration depth on the microhardness distribution [9,10].

Table 3 Additional System Parameters

	Inner Cylinder A	Outer Cylinder B
$H_e(MPa)$	1.20 x10^3	3.27 x10^3
ν	0.33	0.31
m	0.096 – 0.12	0.08

Interfacial Gas (Air) Properties:

$k_{go}(W/mK)$	2.98 x10^{-2}
α_a	2.24
β	1.67
$\Lambda_o(m)$	6.4 x10^{-8}

Compound Cylinder Analysis

In order to compute the joint conductance hence the temperature distribution, we require the contact pressure (1). Similarly, from thermoelasticity the computation of differential contact pressure requires a knowledge of the temperature distribution solution. By an iterative scheme which couples the two solutions, we will determine the contacting pressure in the double tube system, and thus the joint conductance or resistance as required.

First, from linear uncoupled quasi-static thermoelasticity [11], for radial temperature variation only in a long circular cylinder (plane strain, $\epsilon_{zz} = 0$, cylinder ends restrained):

$$\sigma_{rr} = \frac{E}{(1+\nu)(1-2\nu)}[(1-\nu)\epsilon_{rr} + \nu\epsilon_{\theta\theta} - (1+\nu)\alpha\Delta T(r)] \quad (11)$$

$$u = \frac{(1+\nu)}{(1-\nu)}\frac{\alpha}{r}\int \Delta T(r) r dr + B_1 r + B_2/r \quad (12)$$

$$\epsilon_{rr} = \frac{du}{dr}, \epsilon_{\theta\theta} = \frac{u}{r} \quad (13)$$

Elastic Boundary Conditions:

$r = a$ $\quad \sigma_{rr} = P_{INT}$ i) (14)

$r = b$ $\quad \sigma_{rr} = P_c \quad (< 0)$ ii)

$r = b$ $\quad u_A = u_B$ iii)

$r = c$ $\quad \sigma_{rr} = P_{EXT}$ iv)

The upper and lower integration limits in (12) are respectively r and a when $a \le r \le b$, and r and b, when $b \le r \le c$, in the double tube system. The boundary conditions stated are sufficient for elastic contact noting that contacting radial stresses and radial displacements must be uniform at the contact (stresses compressive, displacements positive).

For heat transfer, the governing differential equation in each cylinder can be stated as Laplace's equation (radial temperature variation only),

$$\frac{d^2T}{dr^2} + \frac{1}{r}\frac{dT}{dr} = 0 \quad (15)$$

whose solution is:

$$T(r) = C_1 + C_2 \ell n(r) \quad (16)$$

Thermal Boundary Conditions:

$r = a$ $\quad T_A = T_i$ {without conv.} i) (17)

or

$$r = a \quad h_i(T_A - T_i) = k_A \frac{dT_A}{dr} \quad \{\text{with conv.}\} \quad \text{ii)}$$

$$r = b \quad k_A \frac{dT_A}{dr} = h_j[T_B - T_A] \quad \text{iii)}$$

$$r = b \quad k_A \frac{dT_A}{dr} = k_B \frac{dT_B}{dr} \quad \text{iv)}$$

$$r = c \quad T_B = T_o \quad \{\text{without conv.}\} \quad \text{v)}$$

or

$$r = c \quad k_B \frac{dT_B}{dr} = h_o(T_o - T_B(r)) \quad \{\text{with conv.}\} \quad \text{vi)}$$

From inspection of the heat transfer problem it can be seen that four constants of integration (C_1, C_2, C_3, and C_4) will need to be solved to give the temperature solutions in both cylinders. Similarly, four integration constants (B_1, B_2, B_3, B_4) are required for the thermoelastic stress distributions. Solution of these can be found in Appendix II.

In addition to the thermoelastic stresses caused by heat flow and differential expansion, there was an initial shrink fit radial contact stress P_c^{SH} in the assembly due to cold-fitting ($\delta = 0.0127$ mm radial difference, from Table 2). Hsu and Tam thus reported,

$$P_c^{SH} = \frac{\delta}{b[\frac{1}{E_A}(\frac{b^2+a^2}{b^2-a^2} - \nu_A) + \frac{1}{E_B}(\frac{c^2+b^2}{c^2-b^2} + \nu_B)]} \quad (18)$$

This equation is really an approximation as it should read:

$$P_c^{SH} = \frac{\delta}{b[\frac{1}{E_A}(\frac{a^2+b^2(1-2\nu_A^2)}{b^2-a^2} - \nu_A) + \frac{1}{E_B}(\frac{c^2+b^2(1-2\nu_B^2)}{c^2-b^2} + \nu_B)]} \quad (19)$$

This can be verified by not neglecting the higher order terms in the shrink fit displacement analysis as had been referenced in [6]. Using Eq. (18) as reported with $\delta = 0.0127$ m, and data from Table 2, $P_c^{SH} = 10.598$ MPa. From the corrected Eq. (19), $P_c^{SH} = 12.257$ MPa. The difference is 1.659 MPa, or 241 psi., which represents approximately a 16% increase in the apparent initial contact pressure. As will be seen later in the analysis, this will not change the distribution of results but for a particular flux condition it will shift the location on the curve. General expressions for the radial stresses and displacement are given in Appendix II.

At the contact interface (r=b), the contact stress now becomes:

$$P_c = \frac{E_A}{(1+\nu_A)(1-2\nu_A)}\left[\alpha_A \frac{(1+\nu_A)(1-2\nu_A)}{(1-\nu_A)b^2} \int_a^b \Delta T_A(r) r dr + B_1 - \frac{(1-2\nu_A)}{b^2} \cdot B_2\right] + P_c^{SH} \quad (20)$$

or

$$P_c = \frac{E_B}{(1+\nu_B)(1-2\nu_B)}\left[B_3 - \frac{(1-2\nu_B)}{b^2} B_4\right] + P_c^{SH}$$

Convection heat transfer was not modelled in the analysis of Hsu and Tam's experiment and therefore equations 17 i) and v) were used instead of 17 ii) and vi) to evaluate the thermal integration constants. This was done by prescribing surface wall temperatures similar to those reported from [6, Fig. 3]. The iterative analysis procedure is illustrated in Fig. 3.

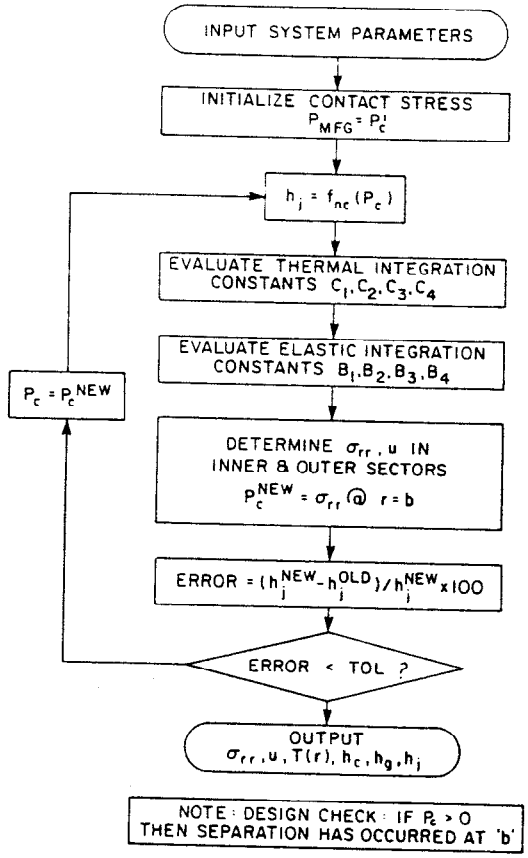

Fig.3 Iterative Algorithm

Comparison of Experimental and Predicted Results

Alternative analytic contact resistance models by Shlykov–Ganin, modified Ross–Stoute [6] and Veziroglu [12] were also studied and compared in the plots. A brief outline of these models is included in Appendix IV. The scheme used for interpretation of the plotted results is as follows:

Sample Set 1 (SS1): Test #1 data with minimum roughness of specimens

$$\sigma_A = 3.048\mu m, m = 0.096$$
$$\sigma_B = 1.270\mu m, m = 0.080$$

Sample Set 2 (SS2): Test #1 data with maximum roughness of specimens

$$\sigma_A = 4.826\mu m, m = 0.12$$
$$\sigma_B = 1.650\mu m, m = 0.08$$

Sample Set 3 (SS3): Test #2 data with minimum roughness of specimens

$$\sigma_A = 0.762\mu m, m = 0.03$$
$$\sigma_B = 1.270\mu m, m = 0.08$$

Sample Set 4 (SS4): Test #2 data with maximum roughness of specimens

$$\sigma_A = 0.940\mu m, m = 0.03$$
$$\sigma_B = 1.650\mu m, m = 0.08$$

Results are illustrated in Figures 4, 5, 6, and 7. Using bulk hardness values given in Table 2, difference in experimental and proposed theory amounts to approximately −25% for the

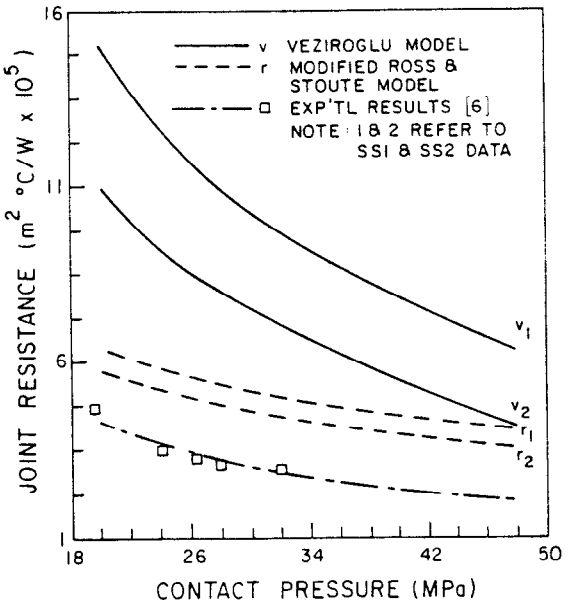

Fig.4 Comparison Between Models and Experimental Results [6] for SS1 and SS2

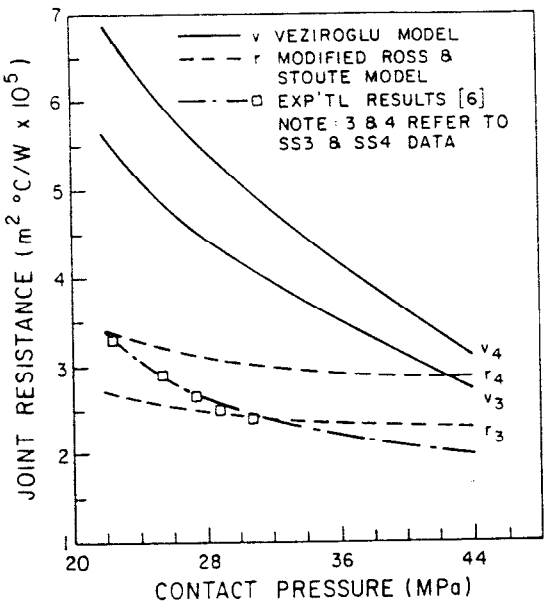

Fig.6 Comparison Between Models and Experimental Results [6] for SS3 and SS4

maximum roughness range (SS2) for test #1, and −40% (SS4) for test #2. In contrast, there is very close agreement between the proposed theory and experimental results to within −3% for the maximum roughness cases (SS2 and SS4), when the Vickers (H_e) microhardness measures are used as reported in Table 3. In comparison the models proposed by Shlykov–Ganin and Ross–Stoute are close for the smooth surface tests (SS3 and SS4) to within ±10 → 30%, but overestimate test #1 results by +30 → 50% (i.e. SS1 and SS2, maximum surface roughness). The model proposed by Veziroglu [12], in both tests, overestimates the results by upwards of +50%.

A list of each of the gap and metal conductance components of the proposed theory is shown in Table 4. For the range of contact pressures studied the major component of the total joint conductance is seen to be the metal (contact) conductance, by approximately an order of magnitude over the gap conductance.

Conversely, the largest resistance component is the gap component. Also, as the smoothness of the specimens increased (for test #2), the overall joint conductance increased by +15 to 20%. Thus, increasing surface roughness has a definite negative effect on contact conductance.

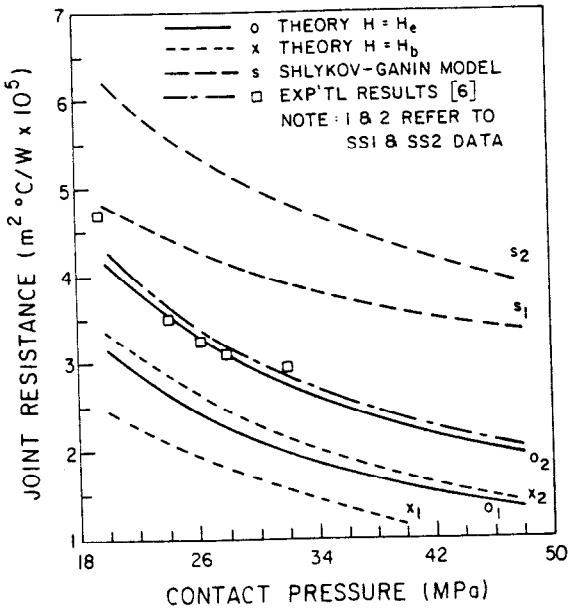

Fig.5 Comparison Between Models and Experimental Results [6] for SS1 and SS2

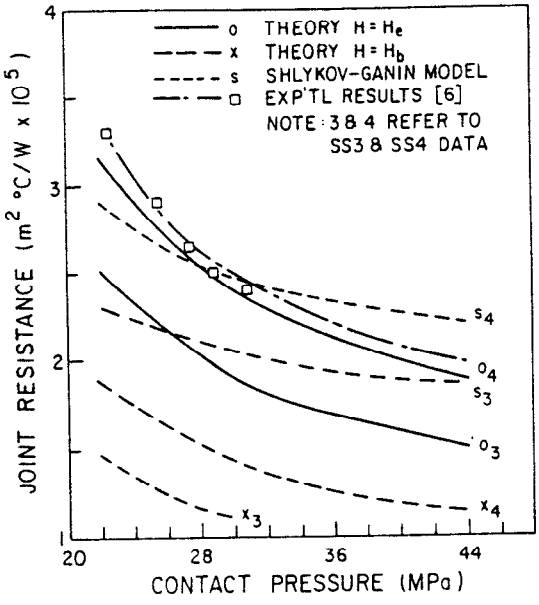

Fig.7 Comparison Between Models and Experimental Results [6] for SS3 and SS4

Table 4 Metal and Gap Conductances

- Test # 1 (corresponds to TCR1 in Ref. [6])

i) SS2) $\sigma_A = 4.83\mu m, \sigma_B = 1.65\mu m, H_e = 1.2$ x10^3 MPa

Contact Pressure (MPa)	Exp'tl h_j (kW/m^2K)	h_c (kW/m^2K)	Proposed Theory h_g (kW/m^2K)	h_j (kW/m^2K)	Abs. % Diff.
22	25.4	23.4	2.71	26.1	2.76
28	30.8	29.1	2.83	31.9	3.56
33	36.4	34.7	2.95	37.7	3.57
40	41.7	40.3	3.17	43.5	4.32

- Test # 2 (TCR2, TCR2X in Ref. [6])

ii) SS4)$\sigma_A = 0.94\mu m, \sigma_B = 1.65\mu m, H_e =$1.8 x$10^3$ MPa

22	30.8	25.2	6.52	31.7	2.92
28	36.8	31.2	6.77	38.0	3.26
33	42.6	37.3	6.98	44.3	3.99
40	47.7	42.8	7.23	50.0	4.82

From the plot of results it is also clearly apparent that the proposed joint conductance theory more closely follows the experimental variation of resistance vs. pressure than the alternative models. Whereas, the Shlykov–Ganin model comes fairly close for the smooth specimens (Fig. 5), it intersects the distribution and does not approximate accurately the trend of the experimental curve. This is also observed for the Ross–Stoute model and the model proposed by Veziroglu [12].

APPLICATIONS TO FINNED-TUBES

As a result of good agreement between experiment and the joint conductance correlations proposed by Yovanovich, a simple analytic approach to finned-tubing will be presented. The tubular fin (edge-fin) to be studied is shown in Fig. 8. The governing equations and boundary conditions for the heat transfer analysis become:

(A) Cylinder $\quad \nabla^2 T_A = 0 \qquad \{T_A = T_A(r)\}$

$$\text{sol'n:} \qquad T_A(r) = C_1 + C_2 \ell nr \tag{21}$$

(B) 1-D Fin

$$\frac{1}{r}\frac{d}{dr}\left[r\frac{d\theta}{dr}\right] - \frac{h}{kt}\theta = 0 \tag{22}$$

where $\theta = T_B(r) - T_o$

$$\text{sol'n:} \quad T_B(r) = T_o + C_3 I_o(\sqrt{Bi}\frac{r}{t}) + C_4 K_o(\sqrt{Bi}\frac{r}{t}) \tag{23}$$

Boundary Conditions:

These are as stated in (17) eq'ns. ii), iii), iv) and vi) where $h_o = h_e = 0$ for the cases studied here.

The four constants of integration (C_1, C_2, C_3, C_4) arising here are listed in Appendix IV, upon solving the boundary conditions. Once again, $C_4 = f_{nc}(h_j) = f_{nc}(P_c)$, requiring an iterative scheme similar to that in Fig. 3 to solve the thermoelastic problem. The stress analysis is similar to that modelled for the compound cylinders with plane strain for the inner tube, except having a plane stress analysis for the fin (treated as a circular disk [11]). The boundary conditions are presented in (14), and the equations and solutions of the necessary constants of integration may be found in Appendix III. The edge-fin to be studied was an aluminum fin on a tubular copper tube. Parameters are listed in Table 5. Variations were conducted on the initial (mfg.) contact pressure (50, 100, 200 psi) as well as on the surface roughness of the materials ($\sigma_1 = 1\mu m, \sigma_2 = .4, .6, .8, 1, 2, 3, 4, m_1 = .07, m_2 = .02, .025, .05, .07, .09, .12, .13$). Outer fluid temperature was 20°C (293K), with $h = 100$ W/m^{2}K ($h_e = 0$). Inner system temperature was varied from 40 to 100°C (313 to 373K), with $h_i = 100$ W/m^{2}K. The interfacial gas was taken as air, with properties as given in Table 3. Results of the analysis are shown in Fig. 9.

Fin Analysis Results

The plots (Fig. 9) show a marked increase in contact resistance as the initial (mfg.) contact pressure was decreased from 1.38 to 0.35 MPa (200 p.s.i. to 50 p.s.i.). Also as the surface roughness increased the joint resistance increased. Very small variation of the joint resistance is seen with respect to flux, i.e. when the initial contact pressure is large enough, thermoelastic expansion pressure has less of an effect and thus could practically be removed from the analysis. Unfortunately the lower initial contact pressures being observed in most light finned-tubing [13] will exhibit a behaviour as shown for $P_c^i = 50$ to 100 p.s.i. Also of interest is the magnitude of the gap and metal conductance terms shown in Table 6. These are seen to be much closer (i.e. same order of magnitude) than was observed in the thick cylinder analysis earlier. It indicates that at low

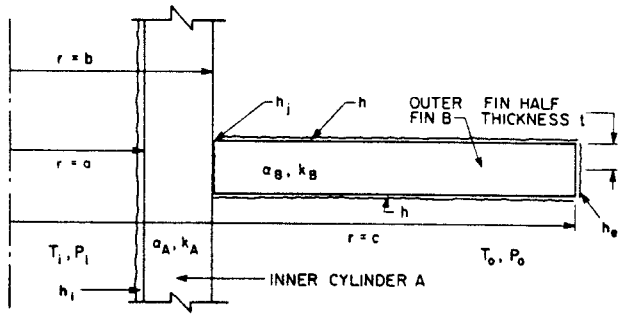

Fig.8 Edge-Fin/Tube System

contact pressures the gap conductance approaches metal conductance, thereby providing an equally likely path for heat to flow. This then supports numerous research endeavours [14,15] into providing a higher conducting film (i.e. liquid, coating) in the gap to increase the governing gap conductance hence decrease the overall joint resistance.

In this fin analysis, the correlation used for h_g was as stated in (3) from ref. [7]. Subsequent work [16,17] has provided a statistical model which is more applicable for free molecular flow to slip regions in the gap. The gap conductance is thus evaluated as an integral [Appendix V] expression. For values of M greater than 2.5 the correlation given in (3) may be used for error less than 1%. For this particular fin analysis M varies from .06 to .16 ($3 \leq Y/\sigma \leq 3.4$) and thus the values shown in Table 6 for h_g are conservative by 10 to 15% indicating an even greater closeness between h_c and h_g at low contact pressures.

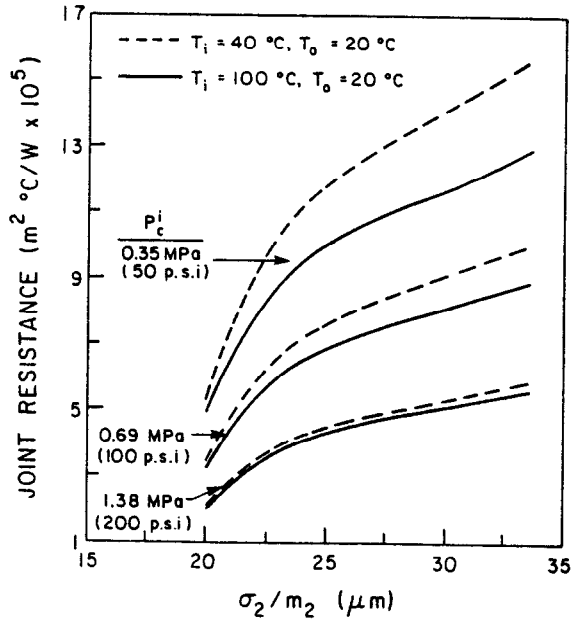

Fig.9 Effect of Variation of Initial Contact Pressure on Joint Resistance for the Edge-Fin/Tube System

Table 5 Edge-Fin Parameters

Copper Tube		Aluminum Fin	
H_c	3.0 x10^3 MPa	H_c	1.2 x10^3 MPa
P_i	0	P_o	0
E_A	1.1 x10^5 MPa	E_B	7.10 x10^4 MPa
α_A	1 x$10^{-5}K^{-1}$	α_B	2.28 x$10^{-5}K^{-1}$
k_A	380 W/mK	k_B	154.9 W/mK
ν_A	0.30	ν_B	0.33
h_i	100 W/m^2K	h	100 W/m^2K

a	4.458 x10^{-3} m	Fin Bi $= ht/k_B$
b	4.763 x10^{-3} m	$= 4.92$ x10^{-5}
c	1.905 x10^{-2} m	
t	7.62 x10^{-5} m	

Table 6 Edge-Fin Conductance Terms

Initial Contact Pressure = 50 psi (.347 MPa)

i) $\sigma_1 = 1\mu m, \sigma_2 = 1\mu m$

Final Contact Pressure (MPa)	h_c (kW/m^2K)	h_g (kW/m^2K)	h_j (kW/m^2K)
0.37	9.00	5.88	14.9
0.40	9.59	5.91	15.5
0.42	10.2	5.94	16.1
0.45	10.7	5.96	16.7

ii) $\sigma_1 = 4\mu m, \sigma_2 = 1\mu m$

0.40	4.87	2.09	6.96
0.44	5.39	2.11	7.50
0.48	5.85	2.12	7.97
0.52	6.28	2.14	8.42

CONCLUSIONS AND RECOMMENDATIONS

The analysis conducted into the thermal joint resistance at the interface has shown that recent correlations developed by Yovanovich [7] verify recently published experimental data [6] for the maximum roughness range of the specimens. It was suggested by Hsu and Tam [6] that existing plane contact models could not be used for predicting the joint resistance in curved surfaces because of thermally induced strain deformation. The results of this study show that the proposed theory agrees very well with experiment if thermoelastic contact stresses are properly developed in the analysis. Other empirical formulas developed by Veziroglu and Ross–Stoute were found to be in significant error by as much as + 50 to 100%. The Shlykov–Ganin model yielded generally closer agreement with test results for very smooth surfaces but with an improper distribution which did not follow the trend of the experimental data. The ba-

sis of the good agreement between the proposed theory and experimental results lies in accurately measuring the key surface parameters: roughness, slope and the effective (Vickers) Hardness distribution. The latter micro-hardness distribution is a correlation of results conducted into various penetration depths, yielding a function dependent on the roughness and slope of the surface [9,10]. General bulk (i.e. Brinell) hardness measures are inadequate in the model but could be used to establish an absolute lower bound on the resistance.

Thermal radiation effects were not included in this analysis but could be easily incorporated into the gap analysis and used in the iterative procedure. The effects of radiation for the cases presented were calculated to be negligible for the temperature ranges used.

The analysis of an edge-fin tube heat exchanger has been developed using the proposed theory for joint resistance. The iterative thermoelastic procedure is based on elastic deformation only and requires the initial (as manufactured) contact pressure of the system. Investigations into the mechanical expansion process of fin-tubes [13] indicate that for a typical system similar to that presented here the initial manufacturing contact pressure range is generally low, usually less than 100 p.s.i. For this range the results of this study show that there is a significant variation of the contact resistance with surface parameters under operating system temperatures. The joint resistance component in a fin-tube system (under mechanical contact) may account for approximately 5% of the total system resistance. This could of course range as high as 10 to 20% depending on the initial contact pressure and actual film resistances. Obviously, a larger variety of studies still need to be conducted.

It is recommended that more studies be conducted into the joint resistance of curved surfaces to further verify the proposed theory, particularly at low contact pressures. Effects such as circumferential vs. axial roughness measures still need to be investigated as well as effects on contact resistance by thermal-cycling.

ACKNOWLEDGEMENTS

The authors, M.M. Yovanovich and T.F. Lemczyk, wish to acknowledge the financial support of the Natural Sciences and Engineering Research Council of Canada under operating grant A7455.

REFAS861.TEX

REFERENCES

1. Gardner, K.A. and Carnavos, T.C., *Thermal Contact Resistance in Finned-Tubing*, Trans. ASME J. Heat Trans., 1960, Vol. 82, pp. 279-293

2. Christensen, R.N., Fernandes, H.V., *Contact and Fouling Resistances in Finned-Tube Heat Exchangers*, ASME Paper No. 83-HT-39, 1983.

3. Eckels, P.W., *Contact Conductance of Mechanically Expanded Plate Finned-Tube Heat Exchangers*, ASME Paper No. 77-HT-24, 1977.

4. Kern, D.Q., Kraus, A.D., Extended Surface Heat Transfer, McGraw-Hill Book Co., 1972, pp. 548-557.

5. Shlykov, Yu.P. and Ganin, Ye.A., *Thermal Resistance of Metallic Contacts*, Int. J. Heat and Mass Transfer, Vol. 7, 1964, pp.921-929.

6. Hsu, T.R., Tam, W.K., *On Thermal Contact Resistance in Compound Cylinders*, AIAA Paper No. 79-1069, AIAA 14th Thermophysics Conference, June 4-6, 1979, Orlando, Florida.

7. Yovanovich, M.M., *New Contact and Gap Conductance Correlations for Conforming Rough Surfaces*, AIAA Paper No. 81-1164, AIAA 16th Thermophysics Conference, June 23-25, 1981, Palo Alto, California.

8. Yovanovich, M.M., Hegazy, A.H., Antonetti, V.W., *Experimental Verification of Contact Conductance Models Based Upon Distributed Surface Micro-Hardness*, AIAA Paper No. 83-0532, AIAA 21st Aerospace Sciences Meeting, January 10-13, 1983, Reno, Nevada.

9. Yovanovich, M.M., Hegazy, A.H., DeVaal, J., *Surface Hardness Distribution Effects Upon Contact Gap and Joint Conductances*, AIAA Paper No. 82-0887, AIAA/ASME 3rd Joint Thermophysics, Fluids, Plasma and Heat Transfer Conference, June 7-11, 1982, St. Louis, Missouri.

10. Hegazy, A.H., Thermal Joint Conductance of Conforming Rough Surfaces: Effect of Surface Microhardness Variation Ph.D. Thesis, Department of Mechanical Engineering, 1985, University of Waterloo, Canada.

11. Boley, B.A., and Weiner, J.H., Theory of Thermal Stresses, John Wiley and Sons, Inc., New York, 1960.

12. Veziroglu, T.N., *Correlation of Thermal Contact Conductance Experimental Results*, Prog. Astron. Aero., Vol. 20, pp. 879-907, Academic Press Inc., New York.

13. Burgers, J.G., M.A.Sc. Thesis in progress, Department of Mechanical Engineering, University of Waterloo.

14. Yovanovich, M.M., Schankula, M.H., Patterson, D.W., *The Effect of Oxide Films on the Thermal Resistance Between Contacting Zirconium Alloys*, American Society for Metals Paper, pp. 106-111, 1983.

15. Cook, R.S., Token, K.H., Calkins, R.L., *A Novel Concept for Reducing Thermal Contact Resistance*, AIAA Paper No. 82-0886, AIAA/ASME 3rd Joint Thermophysics, Fluids, Plasma and Heat Transfer Conference, June 7-11, 1982, St. Louis, Missouri.

16. Yovanovich, M.M., DeVaal, J., Hegazy, A.H., *A Statistical Model to Predict Thermal Gap Conductance Between Conforming Rough Surfaces*, AIAA Paper No. 82-0888, AIAA/ASME 3rd Joint Thermophysics, Fluids, Plasma and Heat Transfer Conference, June 7-11, 1982, St. Louis, Missouri.

17. Zwart, J., Personal Communications, University of Waterloo, 1984, Canada.

APPENDICES

I. Vickers Micro-hardness Distributions ref [10]

Stainless Steel 304

$$H_e = 639.23 d^{-.229}\ \text{kg/mm}^2$$
$$d = 0.9538\left(\frac{\sigma}{m}\right)\ \mu\text{m}$$

For $\sigma = 1.27 - 1.65(\mu m)$, $m = .08$,
avg $H_e = 3.27 \times 10^9$ Pa

Al 2011 (similar to Al 2024 measurements [6])

For the roughness range $3.048 - 4.826(\mu m)$;
SS1 & SS2 ($m = .096 - .12$)

$$\text{estimated } H_e = 1.2 \times 10^9 \text{ Pa}$$

and for the range $0.762 - 0.940(\mu m)$;
SS3 & SS4 ($m = 0.03$)

$$\text{estimated } H_e = 1.8 \times 10^9 \text{ Pa}$$

II. Solutions for Compound Cylinder Analysis

Heat Transfer: $T_A(r) = C_1 + C_2 \ell n\, r$; $T_B(r) = C_3 + C_4 \ell n\, r$

without convection, i.e. prescribed surface temperatures

$$C_1 = T_i - C_2 \ell n\, a$$
$$C_3 = T_0 - C_4 \ell n\, c$$
$$C_4 = \frac{k_A}{k_B} \cdot C_2$$
$$C_2 = \frac{h_j(T_0 - T_i)}{\left(\frac{k_A}{b} - h_j\left(\frac{k_A}{k_B}\ell n(b/c) + \ell n(a/b)\right)\right)}$$

{with convection}

$$C_1 = T_i + C_2\left(\frac{k_A}{h_i \cdot a} - \ell n\, a\right)$$
$$C_3 = T_0 + C_4\left(\frac{-k_B}{h_0 \cdot c} - \ell n\, c\right)$$
$$C_4 = \frac{k_A}{k_B} \cdot C_2$$
$$C_2 = \frac{h_j(T_0 - T_i)}{\left(\frac{k_A}{b} - h_j\left(\frac{k_A}{k_B}\left(\frac{-k_B}{h_0 \cdot c} + \ell n(b/c)\right) + \ell n(a/b) - \frac{k_A}{h_i \cdot a}\right)\right)}$$

Thermoelastic

$$B_1 = \frac{(1+\nu_A)(1-2\nu_A)}{E_A} P_i + \frac{(1-2\nu_A)}{a^2} B_2$$
$$B_3 = \frac{(1+\nu_B)(1-2\nu_B)}{E_B} P_0 + \frac{(1-2\nu_B)}{c^2} B_4 + \frac{\alpha_B}{c^2}\frac{(1+\nu_B)(1-2\nu_B)}{(1-\nu_B)} \int_b^c \Delta T_B(r) r\, dr$$
$$B_4 = \frac{Num\,1}{Den\,1}, \text{ where}$$

$$Num\,1 = \frac{E_A}{(1+\nu_A)(1-2\nu_A)} \frac{(b^2-a^2)(1-2\nu_A)}{a^2 b^2} \left[-\frac{(1+\nu_A)}{(1-\nu_A)} \frac{\alpha_A}{b} \int_a^b \Delta T_A(r) r\, dr - \frac{b(1+\nu_A)(1-2\nu_A)}{E_A} P_i + \frac{b(1+\nu_B)(1-2\nu_B)}{E_B} P_0 + \frac{b\alpha_B}{c^2}\frac{(1+\nu_B)(1-2\nu_B)}{(1-\nu_B)} \int_b^c \Delta T_B(r) r\, dr \right] - \frac{b^2(1-2\nu_A)+a^2}{a^2 b} \left[\frac{E_B}{(1+\nu_B)(1-2\nu_B)} \left\{ \frac{(1+\nu_B)(1-2\nu_B)}{E_B} \cdot P_0 + \frac{\alpha_B}{c^2}\left(\frac{(1+\nu_B)(1-2\nu_B)}{(1-\nu_B)}\right) \int_b^c \Delta T_B(r) r\, dr \right\} - \frac{E_A}{(1+\nu_A)(1-2\nu_A)} \left\{ -\frac{\alpha_A}{b^2}\left(\frac{(1+\nu_A)(1-2\nu_A)}{(1-\nu_A)}\right) \int_a^b \Delta T_A(r) r\, dr + \frac{(1+\nu_A)(1-2\nu_A)}{E_A} \cdot P_i \right\} \right]$$

$$Den\,1 = \frac{E_A}{(1+\nu_A)(1-2\nu_A)} \left\{ \frac{(b^2-a^2)(1-2\nu_A)}{a^2 b^2} \right\} \left(\frac{b^2(1-2\nu_B)+c^2}{bc^2} \right) + \frac{E_B}{(1+\nu_B)(1-2\nu_B)} \left\{ \frac{(b^2-c^2)(1-2\nu_B)}{b^2 c^2} \right\} \left(\frac{b^2(1-2\nu_A)+a^2}{a^2 b} \right)$$

$$B_2 = \frac{Num\,2}{Den\,2}, \text{ where } \quad Num\,2 = \frac{E_B}{(1+\nu_B)(1-2\nu_B)}\left\{\frac{(1+\nu_B)(1-2\nu_B)}{E_B}P_0 - \frac{\alpha_B}{c^2}\left(\frac{\nu_B(1+\nu_B)}{(1-\nu_B)} - (1+\nu_B)\right)\times\right.$$

$$\left.\times\int_b^c \Delta T_B(r)r\,dr + \frac{(b^2-c^2)(1-2\nu_B)}{b^2c^2}B_4\right\} - \frac{E_A}{(1+\nu_A)(1-2\nu_A)}\left\{-\frac{\alpha_A}{b^2}\left(\frac{(1+\nu_A)(1-2\nu_A)}{(1-\nu_A)}\int_a^b \Delta T_A(r)r\,dr + \frac{(1+\nu_A)(1-2\nu_A)}{E_A}P_i\right\}\right.$$

$$Den\,2 = \frac{E_A}{(1+\nu_A)(1-2\nu_A)}\left\{\frac{(b^2-a^2)(1-2\nu_A)}{a^2b^2}\right\}$$

Integral Solutions

$$\int_a^b \Delta T_A(r)r\,dr = \frac{(C_1 - T_{ref})(b^2-a^2)}{2} + \frac{C_2}{2}\left(b^2\,\ell n\,b - a^2\,\ell n\,a + \frac{(a^2-b^2)}{2}\right)$$

-analogous solution for $\int_b^c \Delta T_B(r)r\,dr$.

III. Solutions for Edge-Fin Analysis

Heat Transfer:

$$T_A(r) = C_1 + C_2\,\ell n\,r$$

$$T_B(r) = T_0 + C_3 I_0\left(\sqrt{Bi}\frac{r}{t}\right) + C_4 K_0\left(\sqrt{Bi}\frac{r}{t}\right)$$

$$Bi = \frac{ht}{k_B}$$

$$C_1 = C_2\left(\frac{k_A}{h_i a} - \ell n\,a\right) + T_i$$

$$= C_2 D_1 + T_i$$

$$C_3 = \frac{C_4\left(k_B\frac{\sqrt{Bi}}{t}K_1\left(\sqrt{Bi}\frac{c}{t}\right) - h_c K_0\left(\sqrt{Bi}\frac{c}{t}\right)\right)}{\left(k_B\frac{\sqrt{Bi}}{t}I_1\left(\sqrt{Bi}\frac{c}{t}\right) + h_c I_0\left(\sqrt{Bi}\frac{c}{t}\right)\right)}$$

$$= C_4 D_2$$

$$C_2 = C_4\frac{k_B}{k_A}\left(\sqrt{Bi}\frac{b}{t}\left(D_2 I_1\left(\sqrt{Bi}\frac{b}{t}\right) - K_1\left(\sqrt{Bi}\frac{b}{t}\right)\right)\right)$$

$$= C_4 D_3$$

$$C_4 = \frac{h_j(T_0 - T_i)}{\frac{k_A D_2}{b} - h_j\left(D_2 I_0\left(\sqrt{Bi}\frac{b}{t}\right) + K_0\left(\sqrt{Bi}\frac{b}{t}\right) - D_1 D_3 - D_3\ell n\,b\right)}$$

Thermoelastic:

Cylinder equations (A): as presented in (11)-(12)
Fin equations (B): (circular disk)

$$\sigma_{rr} = \frac{-\alpha_B E_B}{r^2}\int_b^r \Delta T_B(r)r dr + \frac{E_B B_3}{(1-\nu_B)} - \frac{E_B B_4}{(1+\nu_B)r^2}$$

$$u_B = \frac{(1+\nu_B)\alpha_B}{r}\int_b^r \Delta T_B(r)r\,dr + B_3 r + B_4/r$$

$$B_1 = \frac{(1+\nu_A)(1-2\nu_A)}{E_A}P_{INT} + \frac{(1-2\nu_A)}{a^2}B_2$$

$$= F_1 + F_2 B_2$$

$$B_3 = \frac{(1-\nu_B)}{E_B}\left(P_{EXT} + \frac{\alpha_B E_B}{c^2}\int_b^c \Delta T_B(r)r\,dr\right) + \frac{(1-\nu_B)}{(1+\nu_B)c^2}B_4$$

$$= F_3 + F_4 B_4$$

$$B_2 = \left((F_3 - F_1)b - \frac{(1+\nu_A)}{(1-\nu_A)}\frac{\alpha_A}{b}\int_a^b \Delta T_A(r)r\,dr\right)\frac{1}{\left(F_2 b + \frac{1}{b}\right)}$$

$$+\left(\frac{F_4 b + \frac{1}{b}}{F_2 b + \frac{1}{b}}\right)B_4 = F_5 + F_6\ B_4$$

$$B_4 = \frac{Num\,3}{Den\,3}, \text{ where}$$

$$Num\,3 = \frac{E_A}{(1+\nu_A)(1-2\nu_A)}\left(\frac{\alpha_A}{b^2}\frac{(1+\nu_A)(1-2\nu_A)}{(1-\nu_A)}\int_a^b \Delta T_A(r)r\,dr - F_1 - F_5\left(F_2 - \frac{(1-2\nu_A)}{b^2}\right)\right) + \frac{E_B F_3}{(1-\nu_B)}$$

$$Den\,3 = \frac{E_A}{(1+\nu_A)(1-2\nu_A)}\left(F_6\left(F_2 - \frac{(1-2\nu_A)}{b^2}\right)\right) - \frac{E_B F_4}{(1-\nu_B)} + \frac{E_B}{(1+\nu_B)b^2}$$

Integral Solutions

$$\int_b^r I_0\left(\sqrt{Bi}\frac{r}{t}\right) r\,dr = \frac{t}{\sqrt{Bi}}\left(rI_1\left(\sqrt{Bi}\frac{r}{t}\right) - bI_1\left(\sqrt{Bi}\frac{b}{t}\right)\right)$$

$$\int_b^r K_0\left(\sqrt{Bi}\frac{r}{t}\right) r\,dr = \frac{t}{\sqrt{Bi}}\left(bK_1\left(\sqrt{Bi}\frac{b}{t}\right) - rK_1\left(\sqrt{Bi}\frac{r}{t}\right)\right)$$

$$\int_b^r \Delta T_B(r) r\,dr = \frac{(T_0 - T_{ref})}{2}(r^2 - b^2) + C_3\int_b^r I_0\left(\sqrt{Bi}\frac{r}{t}\right) r\,dr + C_4\int_b^r K_0\left(\sqrt{Bi}\frac{r}{t}\right) r\,dr$$

IV. Outline of Alternative Contact Models

note: $\frac{1}{R_j} = \frac{1}{R_c} + \frac{1}{R_g}$

Shlykov & Ganin Model [5,6]

$$\frac{1}{R_c} = \frac{2.1 k_s P_c}{c\sigma_b} \times 10^4 \text{ W/m}^2\text{K}$$

$\sigma_b = 345$ MPa; c = 3 to 5 (high degree of cold work)

$$\frac{1}{R_g} = \frac{2k_{go}}{\sigma_1 + \sigma_2} \text{ W/m}^2\text{K}$$

Modified Ross & Stoute Model [6]

$$\frac{1}{R_c} = \frac{k_s P_c}{0.05\sqrt{\sigma^* H}}\left(\frac{\text{W}}{\text{m}^2\text{K}}\right) \text{ where } \sigma^* = (\sigma_1^2 + \sigma_2^2)/2$$

$$\frac{1}{R_g} = \text{as above (W/m}^2\text{K)}$$

Vezirogl u Model [12]

$$C^+ = \left(\frac{P_c}{H_m}\right)^{\frac{1}{2}}; H_m = \text{Meyer Hardness}$$

$$= 1.04 \times 10^9 \text{ Pa}\,(\text{A}\ell)$$

$$\ell = 3.56(\ell_1 + \ell_2) \text{ if } \ell_1 + \ell_2 < 7\mu\text{m}$$

$$= 0.46(\ell_1 + \ell_2) \text{ if } \ell_1 + \ell_2 > 7\mu\text{m}$$

$$B^+ = 0.335 C^{+0.315(\ell_c/\ell)^{0.137}}; \ell_c = \text{contact length}$$

$$\eta^+ = \frac{k_{go}(k_A + k_B)}{2k_A k_B}$$

$$N_{uc} = 1 + B^+ C^+ / \left(\eta^+ \tan^{-1}\left[\left(\frac{1}{C^+}\right)\sqrt{\left\{1 - \frac{1}{N_{uc}}\right\} - 1}\right]\right)$$

APPENDIX V

Gap Conductance Integral, ref. [16,17]

$$h_g = \frac{k_g}{\sigma}\frac{1}{\sqrt{2\pi}}\int_0^\infty \frac{\exp[-(Y/\sigma - t_g/\sigma)^2/2]}{[t_g/\sigma + M]} dt_g/\sigma$$

where

$$M = \alpha\beta\frac{\Lambda_0}{\sigma}\frac{T_m}{k_0}\frac{P_{go}}{P_g}; t_g = \text{local gap thickness}$$

Zwart [17] gives the following approximation for $Y/\sigma < 4$, which is computationally more efficient than the above;

$$h_g = \frac{k_g}{\sigma}\sqrt{\frac{2}{\pi}}\int_0^3 \frac{\exp\left(-\frac{1}{2}\left(\frac{Y}{\sigma} - u^2\right)^2\right)}{u^2 + M} u\,du$$

This still requires numerical evaluation.

reprinted from
Thermal/Mechanical Heat Exchanger Design – Karl Gardner Memorial Session
PVP-Vol. 118/HTD-Vol. 64
Editors: K. P. Singh, and S.M. Shenkman
(Book No. H00343)

published by
THE AMERICAN SOCIETY OF MECHANICAL ENGINEERS
345 East 47th Street, New York, N.Y. 10017
Printed in U.S.A.